Robust Hand Image Processing for Biometric Application

Jugurta Montalvão[1], Lucas Molina[1], Jânio Canuto[1]

Universidade Federal de Sergipe (UFS), São Cristóvão, CEP. 49100-000.

Abstract A new approach for both hand image segmentation and feature extraction is described. The main advantage of this approach, namely its robustness to low quality images, is illustrated through verification experiments with two public databases: one with scanned images from 50 subjects, and another one with low quality images acquired from 23 subjects, from a conventional webcam. In both cases, features are successfully extracted and good performances are obtained, in spite of image quality. Moreover, the main drawbacks of feature extraction in conventional algorithms are highlighted.

1 Introduction

Hand shape recognition for individual identification/ verification is now a well known biometric modality [1–3]. It is roughly based upon the hypothesis that individuals have different hand geometries (e.g. finger lengths, finger widths, palm area).

Another important hand based biometric approach takes into account palmprints [4,5] instead of contours and/or finger/palm dimensions. Although the fusion of both approaches seems to be a natural trend for hand biometrics, this paper is only concerned with shape based issues.

In spite of the relatively low performance of this kind of biometric scheme, mainly if compared to typical fingerprint or iris based schemes, hand geometry is attractive because of its unobtrusiveness, low-cost and low data storage requirement [6]. Nevertheless, unlike fingerprints, for instance, hand geometry is expected to be more prone to deformations, mainly due to free finger rotations. Consequently, early attempts at individual authentication through hand geometry were mostly based on digital images from hands placed on flat surfaces with fixed pegs carefully placed in order to constrain the hands into a standard position, before hand picture is taken and digitalized [1].

It is also known [2] that, though pegs indeed facilitate image segmentation and feature extraction, it does not totally avoid finger translation/rotation and, unless some kind of image normalization is applied prior to hand-to-hand geometry comparisons, performances can be strongly degraded due to even small mismatchings between parts of such images. Indeed, assuming that mismatchings between images to be compared are a kind of measurement noise, it has been observed that, in some cases, this noise can be much greater than differences between hand geometries from individuals (i.e. useful signal), which are often minute [6].

Moreover, pegs or other positioning devices may deform hand shape if they push the hand skin during data acquisition. For instance, in [1], finger widths just beside pegs are avoided during feature extraction.

Most recent approaches that have appeared in literature claim that they allow "free" hand positioning during acquisition. However, according to what we can infer from database samples presented in [7], [8] and [3], for instance, subjects are somehow induced to place their hands according to a preestablished orientation for the whole hand, into a limited area, from which they are finally free to rotate their fingers, given that fingers do not touch each other. Indeed, this is explicitly mentioned in [2].

A few state-of-the-art works also propose strategies for "contact-free" hand feature extraction, such as in [9, 10]. Though these approaches are more computationally demanding — because hands are free to rove around a 3-D limited space, instead of the usual 2-D flat surfaces — they represent a new paradigm in terms of user acceptance. Unfortunately, they face some segmentation problems that are beyond the scope of this paper. Therefore, in this paper, though some 3-D segmentation problems are briefly mentioned in Section 2, we limit our focus to 2-D hand representation, acquired from flat surfaces.

In spite of the diversity and creativeness of new approaches to process "freely" placed hands, on flat surfaces, there is, at least, a common point among most of

them: they depend upon boundary-following algorithms, even though relatively little attention is paid to this very first step to be done. Consequently, motivated by the lack of robustness of boundary-tracking algorithms, mainly when applied to noisy images of hands with rings or other jewelry, we propose here a new method where no explicit contour tracing algorithms are applied.

In our approach — somehow inspired by the Ensemble Histogram Interval (EIH) approach [11] mainly applied to speech signals, whose main advantage is its robustness against noise —, hand images are scanned column by column (or row by row, alternatively), and fingers are detected by signal frequency analysis.

Thus, the main matter of this work is robustness of hand image processing, which is discussed in Section 2, prior to the description of the proposed method, in Sections 3 and 4. In Section 5, some details concerning databases used in this work are given. In Section 6, experimental results are presented and, finally, we discuss the main issues from the new proposal in Section 7.

2 Robustness Issues

Feature extraction approaches from hand images in [1], [2], [12], [6], [13], [8], [14] and [15], for instance, depend upon common preprocessing steps, namely: foreground segmentation, boundary detection. Moreover, except for [1] and [15], they also depend on contour tracking algorithms. Additionally, after contour tracking is done, corresponding finger and palm contours must be properly segmented.

In most published works, where hand images are scanned with conventional desktop scanners, or pictures are taken under controlled illumination, foreground segmentation is not an important matter. For instance, in [6], both simple clustering and more sophisticated watershed transform-based segmentation were compared through their database, providing equivalent results. Similarly, in [3], after experiments with three clustering algorithms for gray-level threshold search, the authors finally concluded that small variations in the threshold choice do not relevantly affect their final results. Thus, for their database, a range from 65 to 100 (in 256 gray levels) was considered as the threshold choice.

On the other hand, boundary detection and contour tracking seem to be less straightforward matters. Surely, even a simple contour tracking algorithm, whenever it is properly initialized, may do the job correctly. Figure 1 illustrates such a case.

However, algorithms without specific constraints to deal with rings, other jewelry, or even part of the arm are clearly more prone to mistakes and may provide meaningless contours, as it is shown in Figure 2.

In [6], for instance, it is highlighted that delineation of hand contours must be very accurate, since the difference between hands of different individuals are often
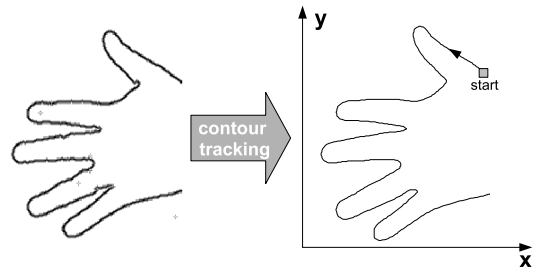

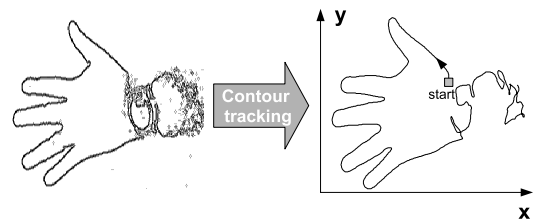**Fig. 1** Successful contour tracing illustration.

Fig. 2 Bad contour tracing illustration.

minute. In fact, the authors pay special attention to the filtering of perturbation due to ring artifacts, however, not enough details are given concerning the boundary-following algorithm used by them.

Similarly, in [2], it is explicitly mentioned that the trace of hand contours is obtained by "a boundary following algorithm". Unfortunately, no further information concerning this algorithm is provided.

In [3], a contour tracking algorithm from [16] was modified: 8 directions were considered instead of 4. This adaptation was not justified in the paper but we believe that it may have been motivated by robustness issues, to avoid bad contours.

To get some experimental insights concerning this issue, we also adapted a simple tracking bug algorithm to thinned hand contours in our own low-quality database (the BioChaves database, see Section 5 for further details). But first, we manually removed wrist and arm from each original image (a typical example is show in Figure 2), in order to get only fingers and palm contour, as it is shown in Figure 1. Still, the algorithm was carefully initialized with a start point corresponding to the thumb contour. It is worth noting that to do so, some initial information concerning hand position and orientation is necessary. However, in spite of this highly favorable setup, in our experiment with low quality images, we obtained 12 bad contours, out of 115 images.

Furthermore, once hand contours are properly obtained, in most approaches, it is necessary to estimate which part of the contour corresponds to each finger, so that each finger can be translated/rotated prior to metric comparisons. In both [2] and [13] very similar algorithms based on contour curvature to detect fingertips and valleys between fingers are used. However, from Fig-

ure 2(a) in [2], it is easy to infer that correct fingertip and valley detection depends upon a threshold to be set to a limited value interval — high thresholds may cause false detection of tips/valleys, whereas small ones may cause non-detection of actual tips/valleys[1].

We applied the algorithm proposed in [2] to our database and we indeed observed that this limited threshold interval, illustrated in Figure 3, is a clear drawback of this approach, in terms of robustness.
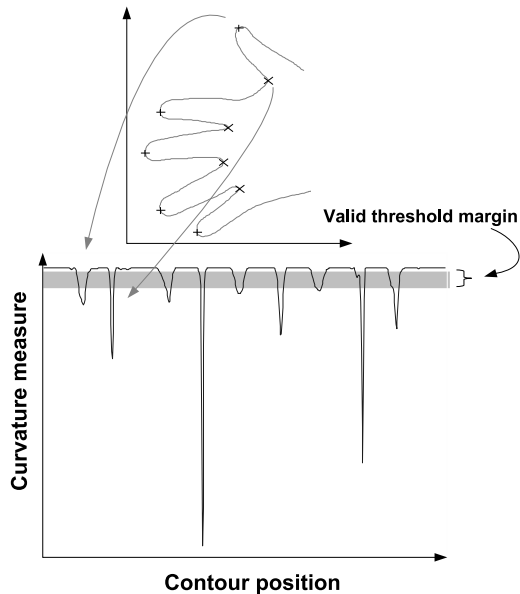

Fig. 3 Curvature based method for finding fingertips and valleys between fingers.

In order to cope with this lack of robustness, in [13], a Gaussian (low-pass) filter is applied to the signal corresponding to the contour curvature index, therefore, providing a larger range for a suitable threshold. Nevertheless, none of them study the risk of tips/ valleys detection failing, in spite of the importance of the success of this step for the whole algorithm, in both cases. That is to say that, if a single valley is missed, for instance, all features detected afterwards are likely to be meaningless.

Yoruk et al. [6] have experimented with the same approach based on the curvature of the contour for detection of tips and valleys, but they observed that "this technique was rather sensitive to contour irregularities, such as spurious cavities and kinks, especially around the ill-defined wrist region". Consequently, they proposed a more robust alternative, based on the radial distance from contour points to a reference point around the wrist region.

---

[1] Some papers, such as [3], don't provide an explanation for either how the arm is separated from the hand, or how finger tips are detected.

Unfortunately, the reference point, defined as the first intersection point of the major axis (the largest eigenvector of the hand inertial matrix) with the wrist line, depends on the definition of the wrist line, not provided in their paper. Nevertheless, we tried the approach by assuming that the reference point is the closest intersection point toward the wrist (note that a previous knowledge about finger orientation is necessary in this case). But, as it is illustrated in Figure 4, the reference point found in this way is not a robust parameter, at least for images in our database, though the approach proposed in [6] is possibly suitable for images taken from conventional scanners, as in their work, where hands are easily segmented from the foreground, excluding parts of the arm.
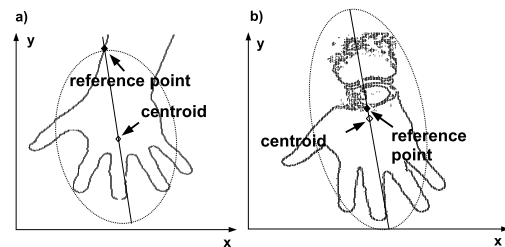

Fig. 4 Finding reference points according to the strategy proposed by Yörük et al. [6].

Finally, even in contact-free hand geometry techniques, such as [10] and [9], hand segmentation is a crucial concern. In [10], for instance, though feature point extraction is performed in a fairly clear imaging background, the authors remark that it (automated feature extraction) remains a "very challenging process". Indeed, in spite of their powerful approach based on projective invariants, in order to get hand boundary properly detected, they need an application-tuned Canny edge detector, two thresholding steps, one being with hysteresis, and a morphological erosion. They also apply a zero-crossing technique to identify edge pixels during finger seam detection. Again, a third threshold is necessary to filter trivial edges.

Similarly, in [9], where a 3-D segmentation is done through the fitting of a Gaussian Mixture Model to the detected points, the convergence of the iterative Expectation-Maximization procedure relies on good initial parameter values. Therefore, in order to cope with the risk of wrong convergency, which is analogous to 2-D region segmentation through clustering, the authors exploit prior knowledge of the body geometry. Nonetheless, even with this application-tuned solution, after hand points are segmented, the authors declare that hand silhouette is not reliably estimated. Consequently, they follow a more elaborate procedure instead, based on the distance transform, which provides the smallest distance from each pixel to the noisy hand boundary. As a result, both palm

center and approximated radius are estimated without contour tracking.

Motivated by the former observations, we propose a new method based on the following straightforward hypothesis:

- In behalf of robustness, explicit contour tracking algorithms are to be avoided.
- In most hand images, three or four fingers are almost parallel and detection based on this parallelism is less prone to mistakes.
- Doing multiple trials of simple detection tests is a straightforward recipe for robust strategies. More specifically, our approach is directly motivated by results from the application of the Ensemble Histogram Interval (EIH) [11] on speech signals, and by its robustness against noise.

We highlight that the application of this method is limited to 2-D hand images, or 2-D projection of 3-D models.

3 Image Preprocessing

Before application of the proposed method itself, a simple two-step pre-processing must be considered for each hand image. Pictures are assumed to present a single left hand image. Whenever the background is roughly uniform, a single threshold should be applied in order to provide a two level representation, where hand (foreground) pixels are coded in black and background pixels, in white. Figure 5 illustrates this first preprocessing step.
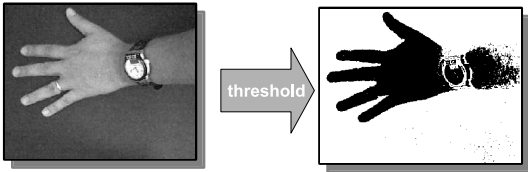

Fig. 5 Preprocessing - step 1: thresholding.

From our database, three color channels – red, green and blue – from each hand picture are available, with intensity levels ranging from 0 (lowest) to 255 (brightest). For our database, enough contrast between foreground (hand) and background was observed from the red channel, which was systematically taken as preprocessing input. Then a static intensity threshold equal to 100 was applied to provide the two-level matrix, where each entry corresponds to a image pixel, whose gray level attribute is 0 (black foreground) whenever red channel intensity is above threshold, or 255 (white background) otherwise.

HSV color space representation prior to background segmentation was also tested, but it did not improve segmentation results. As far as we can understand this

result, it is probably due to the strong amount of red present in the targeted foreground, the human skin. Nonetheless, we highlight that, depending on the background color, perceptual color space, such as HSV, would provide better results. In any case, even in RGB space, we did not optimize discriminability between foreground and background. Instead, we chose channel R for simplicity. Besides, it is clear that we could improve foreground segmentation by using better illumination or even another, more elaborated setup for hand image capture. Nonetheless, the noisy foreground segmentation we obtained is rather welcome in this work because it highlights the robustness of the main part of our approach, which is aimed at replacing boundary-following algorithms.

This two-level matrix is then low-pass filtered and, from the resulting matrix, $\mathbf{M}$, two discrete gradient matrices are obtained, namely $\mathbf{D}_x$ and $\mathbf{D}_y$, according to:

$$\mathbf{D}_x = \mathbf{M} * \mathbf{H} \tag{1}$$
$$\mathbf{D}_y = \mathbf{M} * \mathbf{H}^T \tag{2}$$

where symbol $*$ stands for 2D discrete convolution, T stands for matrix transposition and

$$\mathbf{H} = \begin{bmatrix} +1 & +1 & 0 & -1 & -1 \\ +1 & +1 & 0 & -1 & -1 \\ +1 & +1 & 0 & -1 & -1 \\ +1 & +1 & 0 & -1 & -1 \\ +1 & +1 & 0 & -1 & -1 \end{bmatrix}$$

is the low-pass filter mask.

Then, intensity gradient, $\mathbf{G}$, can be obtained as in Equation 3.

$$\mathbf{G}(i,j) = \mathbf{D}_x(i,j)\mathbf{u}_x + \mathbf{D}_y(i,j)\mathbf{u}_y \tag{3}$$

where $\mathbf{u}_x$ and $\mathbf{u}_y$ are orthonormal vectors.

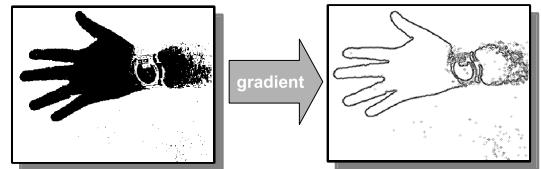Figure 6 illustrates this second pre-processing step by showing $|\mathbf{G}|$ as a gray bitmap.

Fig. 6 Preprocessing - step 2: boundary detection.

4 Proposed Method

4.1 Step one: column-by-column scanning

First, a compensation factor $\mathbf{C} = \cos(\mathbf{\Omega}(i,j))$ is computed for each image pixel, according to Equation 4,

where $\mathbf{\Omega}(i,j) = \angle\mathbf{G}(i,j) - \pi/2$, as illustrated in Figure 7.

$$\mathbf{C}(i,j) = \frac{\mathbf{D}_y(i,j)}{(\mathbf{D}_x(i,j)^2 + \mathbf{D}_y(i,j)^2)} \qquad (4)$$

Then, assuming that matrix $\mathbf{M}$ represents a single left hand image with fingers oriented from right to left, $\mathbf{M}$ is then scanned column-by-column, so that whenever a Θ_{gray} level (threshold) crossing is detected, the corresponding line, j, is recorded along with its column, i.

Each thus detected pixel position, (i,j), along with the corresponding parameters $\mathbf{L}(i,j)$ and $\mathbf{C}(i,j)$, are given as inputs to a list of all points sequentially detected, column-by-column, through the whole matrix (bitmap) $\mathbf{M}$.

Let $P_n = (i_n, j_n)$, $n = 1, \dots, N$ be the whole set of points sequentially detected from the leftmost column to the rightmost one. Then, a rough but biased finger and/or palm width estimation, in pixels, is provided by

$$L(i,j) = j_{m+1} - j_m$$

where m only corresponds to points P_m associated to high-to-low Θ_{gray}-gray level crossings (presumably, a lower boundary of a finger/palm).

Clearly, finger/palm width estimation $\mathbf{L}(i,j)$ strongly depends on the finger/palm rotation. That is to say that fingers and/or palm, not horizontally oriented, do provoke biased higher $\mathbf{L}$ values.

To compensate for this bias, $\mathbf{L}(i,j)$ must be multiplied by the compensation factor $\mathbf{C}(i,j)$, according to the illustration in Figure 7.
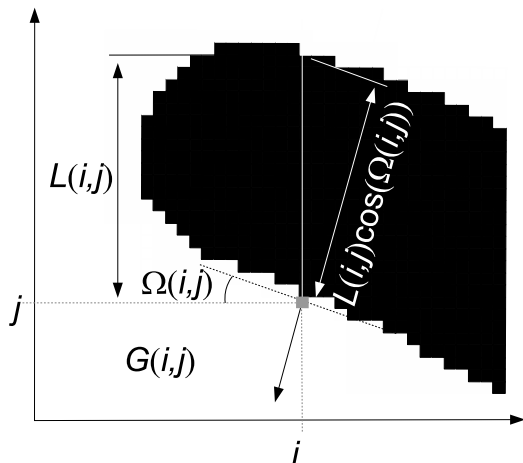

Fig. 7 Method illustration — step one.

4.2 Step two: spectral detection of quasi-parallel fingers

Alternatively, an equivalent representation of detected points and their corresponding parameters is provided by the following vectors:

– $x(m)$: column index, i, where the m-th high-to-low Θ_{gray} crossing was detected. Note that columns are scanned from left ($i = 1$) to right.
– $y(m)$: row index, j, (down-up) corresponding to the m-th detected high-to-low Θ_{gray} crossing.
– $l(m)$: corresponding compensated width, i. e. $l(m) = L(i,j)C(i,j)$.
– $c(m)$: corresponding compensation factor, i. e. $c(m) = C(i,j)$.

Thanks to this representation, $y(m)$ can be seen as an 1D signal and, given that three or four fingers are expected to be horizontally oriented, $y(m)$ is likely to present a quasi-periodic behaviour through columns that intercept those fingers, whose period is 3 or 4, respectively, i.e. $y(m) \approx y(m+3)$, throughout columns that intercept 3 quasi-parallel fingers, and $y(m) \approx y(m+4)$, for 4 quasi-parallel fingers. Figure 8 illustrates a segment of signal $y(m)$ in which a quasi-periodicity is observed.
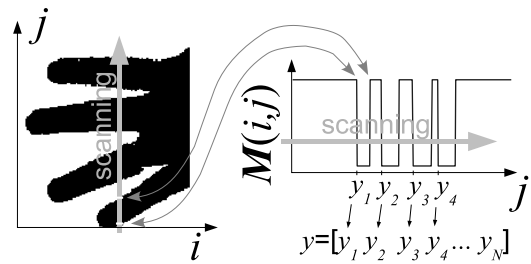

Fig. 8 Quasi-periodicity illustration.

Therefore, much like a barcode scanner, in this specific step, the method runs throughout columns looking for three or four barely parallel and equally spaced bars, corresponding to fingers.

Note, however, that approximation $y(m) \approx y(m+T)$ is also true for any $T > 1$ whenever $y(m)$ remains almost constant (DC signal). Consequently, detection of intervals for m where $y(m)$ is quasi-periodic with $T = 3$ or $T = 4$ is a crucial task accomplished by tuned filters, where each filter, tuned at period $T = 1, 2, 3,$ or 4, respectively corresponds to the nonlinear mapping given in Equation 5.

$$a_T(m) = \sum_{k=m}^{m+10} \left| \frac{y(k+T) - y(k)}{y(k)} \right| \qquad (5)$$

where $y(k)$ is always a positive non-null row counter.

Once signals $a_1(m)$ to $a_4(m)$ are available, a simple logic test indicates the interval, for variable m, in which the signal $y(m)$ is more likely to correspond to quasi-parallel finger detection. This test, given by

$$a = \begin{cases} 1, \text{if}((a_1 > A) \cup (a_2 > A)) \cap \\ \quad ((a_3 < A) \cup (a_4 < A)) \\ 0, \qquad \text{otherwise} \end{cases}$$

(where threshold $A = 0.01$ was set experimentally), looks for quasi-periodicity of $y(m)$, while it also avoids constant and quasi-constant signals.

It is worth noting that threshold $A = 0.01$ only depends on the noise level of the image, and we experimentally observed that 0.01 seems to be a suitable value even for low quality images, as in our database.

Figure 9 illustrates how $y(m)$ is processed in order to provide a flag signal $a(m)$, which equals one (true) for values of m corresponding to columns where quasi-parallel fingers are detected.
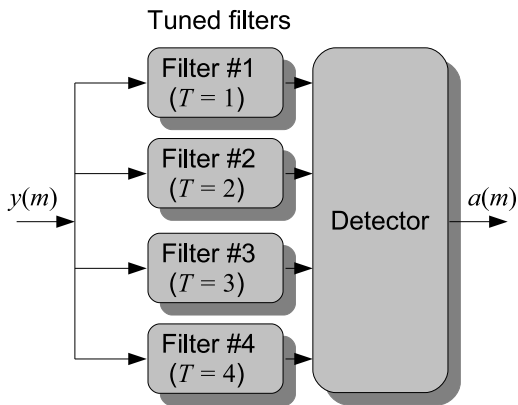

Fig. 9 Tuned filters for quasi-periodicity detection.

Figure 10 gives an illustration of how signal $a(m)$ is obtained throughout logic operations.

4.3 Step three: average finger width estimation and hand region delimitation

Average finger width is estimated according to Equation 6.

$$\bar{L} = \frac{\sum_{m=1}^{M} l(m)a(m)}{\sum_{m=1}^{M} a(m)} \tag{6}$$

where M stands for the length of vector y.

This average finger width, $\bar{L}$, plays a central role in the following steps. Based on this parameter, fingers and palm are segmented from the arm, a watch or whatever is not relevant to the process.

Indeed, from $\bar{L}$ and the average column

$$\bar{X} = \frac{\sum_{m=1}^{M} x(m)a(m)}{\sum_{m=1}^{M} a(m)}$$

and based on typical hand proportions, we define an interval of image columns in which we expect to find all fingers and palm, i.e.:

$$X_{min} = \bar{X} - 3\bar{L}$$
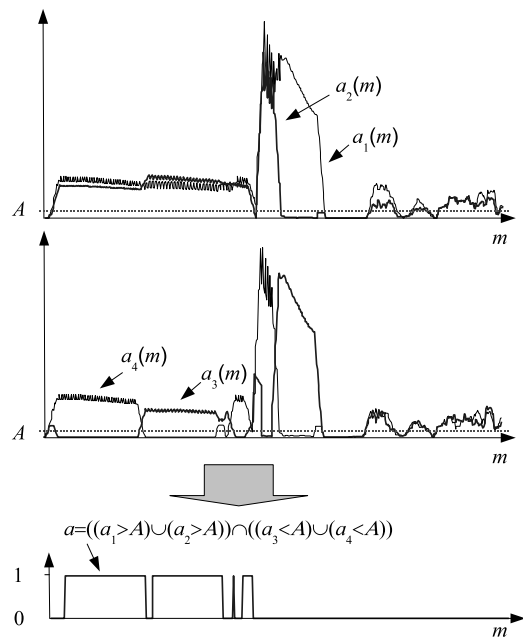
and

$$X_{max} = \bar{X} + 6\bar{L}$$

Fig. 10 Flag (logic) signal indicating quasi-parallel finger detection.

define a interval for x (column index) which should encompass all fingers and palm, while it avoids wrists, according to average hand proportions we estimated from our database. We highlight that these proportions roughly remain constant for normal hand shapes[2].

Similarly, an expected average palm width is defined as $\bar{Pa} = 4\bar{L}$. These two dependent average measures, $\bar{Pa}$ and $\bar{L}$, are then used to filter $x(m)$ between X_{min} and X_{max}, according to their associated width attributes.

For the sake of clarity, we define feature vectors as:

$$\mathbf{f}(m) = [x(m) \; y(m) \; l(m) \; c(m)]$$

Accordingly, a filter is applied so that only feature vectors, $\mathbf{f}(m)$, inside the interval for m corresponding to columns from X_{min} to X_{max}, whose width attributes, $l(m)$, are in the interval from $0.5\bar{L}$ to $1.5\bar{Pa}$, are transmitted to the next algorithm step.

4.4 Step four: palm segmentation

After hand segmentation and filtering based on average finger width, selected feature vectors are expected to represent only fingers and palm. Consequently, widths should be roughly characterized by a bimodal distribution: low widths for fingers and high widths for palm. Thus, even a simple clustering algorithm would be able to provide palm segmentation.

---

[2] Indeed, similar standard hand proportions are frequently used by art students, for instance.

Nevertheless, for robustness concerns, we apply here a simple threshold based selection, i.e., feature vectors whose width attributes are greater than $3\bar{L}$ are segmented as palm features. Note that this threshold is adaptive, for it depends on $\bar{L}$.

4.5 Step five: finger segmentation

Initially, feature vectors whose width attributes lie between $0.5\bar{L}$ and $1.5\bar{L}$ are segmented as fingers.

The whole set of feature vectors thus segmented as fingers is to be properly clustered and labeled as thumb, index, middle, ring, or little finger. For this specific task, we use a simple but robust sequential clustering algorithm, which can be summarized as follows:

1. Initialize 9 clusters with null feature vectors.
2. Through columns corresponding to segmented fingers, from left to right, do:
   2.1 Compute the absolute difference between attribute $y(m)$, (row) from each feature vector, and the corresponding feature from the last input in each cluster.
   2.2 If the minimum absolute difference is less than $\bar{L}/2$, then accept this feature vector as a new input to the corresponding cluster (closest one).
   2.3 Otherwise, if there is still a cluster with only null vectors, accept the new feature vector as the first non-null input to it (i.e., start a new non-null cluster). In case all clusters are already fulfilled with non-null entries, then stop.
3. Sort all clusters according to their cardinality and take the five biggest ones.
4. Sort these 5 biggest clusters according to the average y attribute (centroid row, $\bar{y}$)
5. From the highest to the lowest $\bar{y}$, corresponding clusters are associated, respectively, to thumb (1), index (2), middle (3), ring (4), or little (5) finger.

Thus, from each hand picture, 6 sets of non-null feature vectors are extracted, namely: F_0, from palm, F_1, F_2, F_3, F_4 and F_5 from thumb, index, middle, ring, and little finger, respectively.

Finally, in agreement with the study presented in [2], concerning the sub-segmentation of fingers into smaller parts to improve distinctiveness between individuals, sets F_k, $k = 1, \ldots, 5$, are split into subsets $F_{k,1}$, $F_{k,2}$, $\ldots$, $F_{k,NP}$, where NP stands for the number of finger slices (subsets) to be considered.

4.6 Step six: hand proportions estimation

A final step for feature extraction is the estimation of finger/palm length and average width, which can be easily obtained from subsets $F_{k,m}$, $0 \leq k \leq 6$, and $1 \leq m \leq NP$, for $k \neq 0$. Indeed, average widths, $w_{k,m}$, are thus estimated as the mean of all width attributes in subset $F_{k,m}$, whereas finger/palm length, $h_{k,m}$, is simply the cardinality of the corresponding cluster — i.e. the number of columns that intercept each finger or palm — divided by the averaged c of the cluster. This division compensates for cardinality dependency upon finger/palm rotation.

We highlight that, alternatively, when pictures of hands to be compared are taken with different resolutions (in terms of pixel per inch, for instance), all estimated proportions h and w, here expressed in number of pixels, can be divided by $\bar{L}$ in order to provide a dimensionless set of measures.

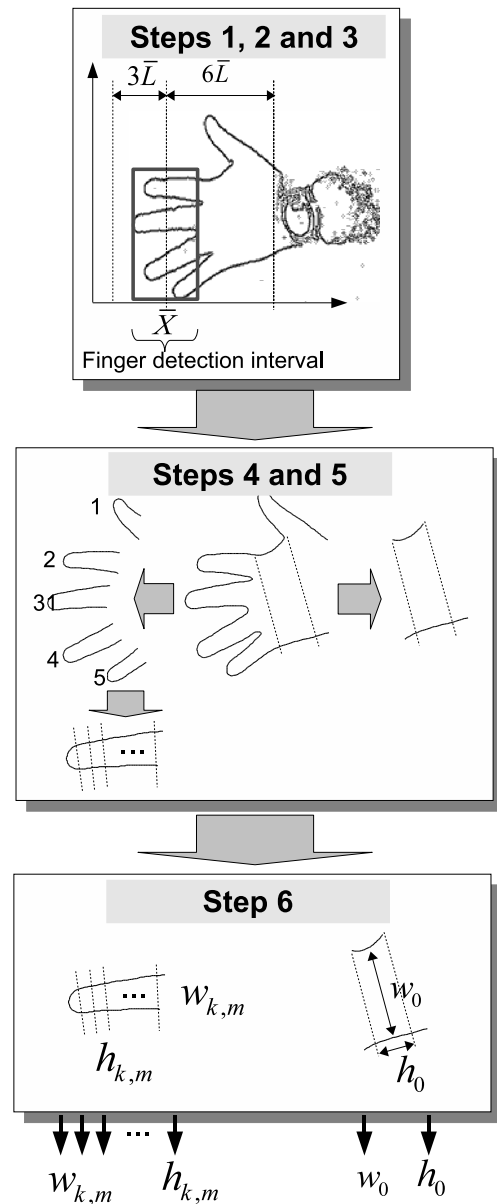Figure 11 provides an overall illustration of the six steps for feature extraction.

Fig. 11 Whole method illustration.

4.7 Hand proportions comparison

Let h^u, w^u represent hand features from the u-th picture in the database, whereas h^v, w^v, represent those from the v-th picture. A simple comparison between hand shapes is provided by the summation of absolute differences between corresponding features, i.e., the Manhattan distance between features [17].

5 Data Acquisition

Two databases were used in experiments with the proposed method:

a) the BioChaves hand database[3] ,
b) and the GPDS [3] database, downloaded from the Internet in December 2006.

In the BioChaves database, hand pictures were taken with a conventional low cost webcam, attached to a support over a black background. Figure 12 illustrates this setup, where we can observe that 6 white paper strips, over the black background, roughly orientate hand positioning. That is to say that, in the BioChaves database, hands are not freely positioned, though no pegs were used. Furthermore, images were acquired in low resolution: 288 rows per 352 columns, and illumination provided just by the fluorescent lamps already present in our laboratory.
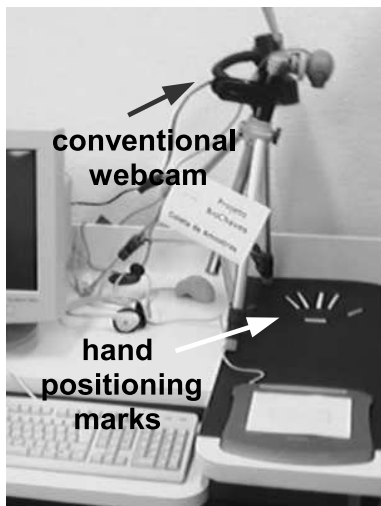

Fig. 12 Image acquisition setup.

As indicated in Figure 13, we got 5 images per subject, from 23 subjects. After each new picture, subjects were asked to remove his/her hand from the setup and replace it a few seconds later.

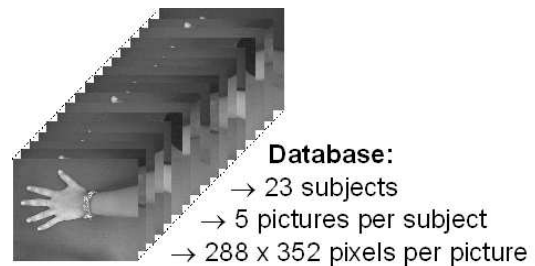[3] Database available for download at www.ufs.br/biochaves.

Fig. 13 Database illustration.

Additionally, 10 out of the 23 subjects were asked to come back at least one month later, and provide 5 more samples (images) from the same hand. This second set of images will be referred to as the second session, in Section 6.

In the GPDS database, images were acquired with a typical desk-scanner using 8 bits per pixel (256 gray levels), with a resolution of 1403 rows per 1021 columns, consisting of 10 different acquisitions per subject, from 50 subjects. The number of sessions in not given.

6 Experimental Results

Three experimental results are presented here. One with the GPDS database of scanned images of right hands, and two with the BioChaves database, with left hand images from a conventional webcam.

As explained in Section 3, the very first algorithm we implemented to test the new method is adapted to process left hand pictures (as in Figure 5), in which fingers are oriented from right to left, whereas the thumb is in the higher part of the image. However, in the GPDS database, only scanned images from right hands are provided, with fingers oriented upward and thumb on the right side. Fortunately, a very simple adaptation was possible by a 90 degrees counterclockwise rotation of such images.

Therefore, we highlight that images from BioChaves (from a webcam) and GPDS (scanned) databases were taken from opposite sides of hands. Moreover, hand positioning in the BioChaves database was partially constrained by white strips over the black background, as it is shown in Figure 12. In all experiments, parameter NP was set to 9 (i.e, $NP = 9$. See Subsection 4.5 for further details).

For the first experiment, each image (out of 10 per subject) was compared to all other images in the GPDS database. Thus we tried to simulate a single picture enrollment *versus* a single picture interrogation. Whenever the score computed with images from the same subject is above a given threshold, a false rejection is registered, whereas a false acceptation is registered whenever scores from different subjects are below the same threshold.

In Figure 14, it is possible to observe both False Acceptation Rate (FAR) and False Rejection Rate (FRR) dependence on the decision threshold, along with two distance histograms: one from the same subject (left histogram), and another from different subjects (right histogram). The threshold which provides Equal Error Ratio (EER - the operational point where FAR equals FRR) is also indicated.
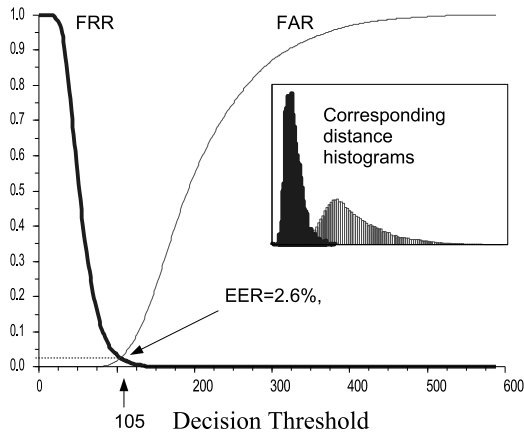

Fig. 14 FAR and FRR variation from the GPDS database.

In order to provide another point of view, Figure 15 presents a Receiver Operating Character (ROC) Curve for the same experiment.
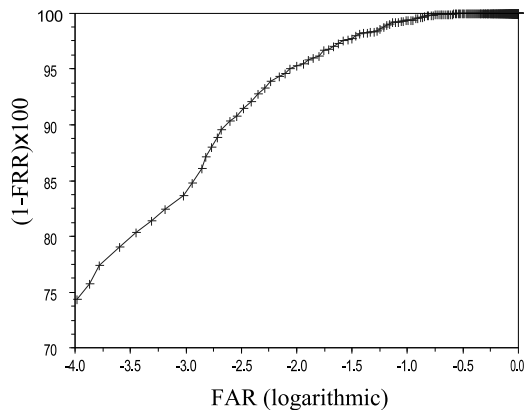

Fig. 15 ROC curve from the GPDS database.

As a second experiment, the same one-sample enrollment/interrogation simulation was done with the BioChaves database. As it was mentioned in Section 2, we were unable to successfully process all images in our low quality database necessary for estimating a vectorial representation of the hand contour (a basic step for feature extraction in most approaches). By contrast, all images were successfully and correctly processed and features automatically extracted with our new proposed method.

Figure 16 presents the experimental result obtained from the BioChaves database, with 5 samples (images) from each subject, and 23 subjects.
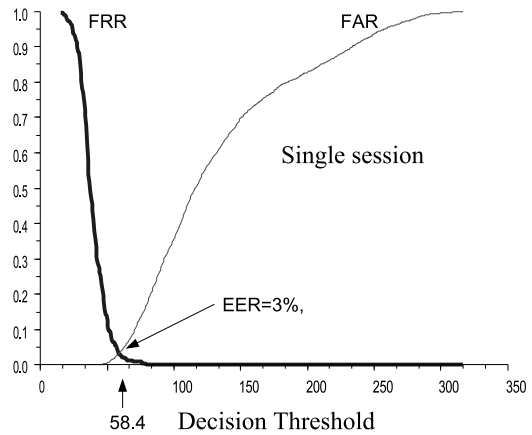

Fig. 16 FAR and FRR variation from the BioChaves database.

In this experiment, an $EER \approx 3\%$ was obtained, quite close to the $EER \approx 2.6\%$ in spite of the difference between data acquisition setups. Moreover, as expected, the lower quality of the BioChaves images leads to a lower performance, in terms of EER. We should observe, however, that EER corresponding thresholds depend on image resolution, for distances between features are measured in number of pixels.

Finally, in the GPDS database it is not mentioned whether images were acquired during a single session (i.e., all images per subject acquired at once) or otherwise. Therefore, in order to simulate a situation in which interrogation (still with a single image) is done at least one month after enrollment, we asked 10 subjects (out of 23) to provide 5 more samples, at least one month after the first session. Then, we again did the one-sample enrollment/interrogation experiment. However, in this case, only comparisons between samples from different sessions were allowed. It roughly corresponds to a simulation of interrogation done more than one month after enrollment. Figure 17 shows the result in terms of FAR and FRR, along with the corresponding EER.

In Figure 18, we can compare performances with samples from one or two acquisition sessions.

7 Discussion and Conclusions

A new method for feature extraction from hand images was proposed. It was mainly motivated by the lack of robustness of most strategies based on contour tracking algorithms.

Inspired by the well-known robustness of the Ensemble Histogram Interval (EIH) processing against background noise, mainly applied to feature extraction from
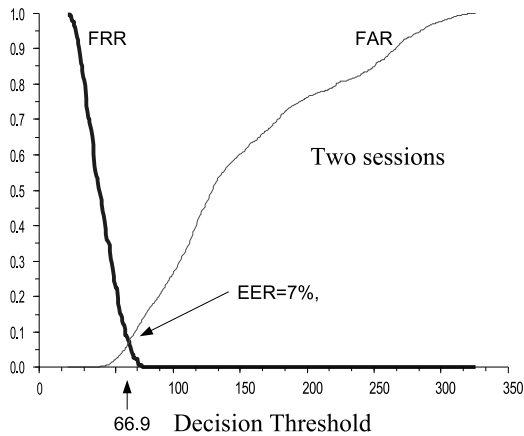
Fig. 17 FAR and FRR variation from the BioChaves database — two sessions.
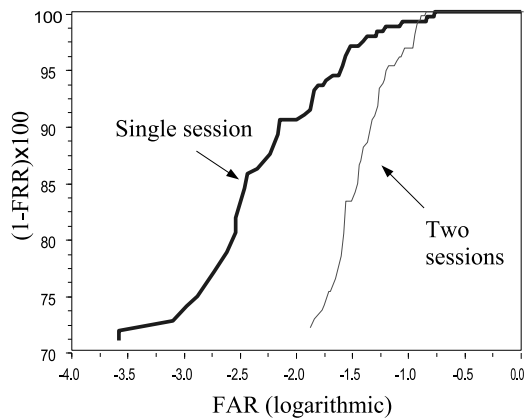

Fig. 18 ROC curves from the BioChaves database.

speech signals, we proposed a new method where hand images are scanned column by column (for hands horizontally oriented) and fingers are detected through an interval between (gray) level crossing analysis, as in EIH based algorithms.

The strength of this kind of approach is partially due to the repetition of simple tests. This multiplicity of tests tends to reduce the influence of individual errors caused by noise.

For the specific case of hand image processing, it is particularly useful for quasi-parallel finger detection, even when subjects are wearing rings, for the multiplicity of periodicity tests (one to each column) improves the probability of finding fingers, from which average width (i.e. finger width) estimation plays a central role in the method. A few experimental verification results are presented as illustrations of the performance of this new method, and performances are comparable to those presented in [2], which is a quite expected result, for the features we use here are the same, i.e. fingers and palm width and height, though the extraction methods are rather different.

We further highlight that, once hand contours, finger tips and valleys between fingers are correctly detected, we do not expect our method to outperform, for instance, results presented in [2], in terms of EER. However, we claim that, whenever there is a high fail rate of finger tips/valley detection, our approach provides a reliable alternative method with competitive performance.

Moreover, through experimental results from databases prepared with very different setups, we observe a consistent performance, roughly expressed by EER close to 3%, with data from a single acquisition session. We further highlight that all images, in both databases, were correctly processed, with the very same algorithm. That is to say that no algorithm adaptation was necessary other than the 90-degree counterclockwise rotation of images from the GPDS database.

For the last experiment, in which two data acquisition sessions were used, at least one month apart from each other, a lower performance was obtained, as expected. Indeed, some of the subjects that took part in this experiment had their hand shape clearly changed from one session to another. For instance, one of them was a pregnant woman whose weight slightly changed during this period. Certainly, we believe that this worse result is much more realistic for practical applications of the method.

Now, we are just paving the route to analyzing the influence of each finger on hand shape recognition, and to improving the method performance through fusion strategies. A more straightforward future work, also in preparation, is the adaptation of the method to any possible hand orientation.

In spite of the smallness of our database (BioChaves), we tried to compensate for this drawback by making it available for download at www.ufs.br/biochaves, and thus allow further comparisons between the results reported here and performances from other strategies. Furthermore, a simple routine, in Scilab code [18], for feature extraction from grayscale bitmaps, according to the new method proposed in this paper, is also available for download at the same website.

Acknowledgments

References

1. R. Sanchez-Reillo, C. Sanchez-Avila, A. Gonzalez-Marcos, Biometric identification through hand geometry

measurements, IEEE Transactions on Pattern Analysis and Machine Intelligence 22 (10) (2000) 1168–1171.

2. W. Xiong, K.-A. Toh, W.-Y. Yau, X. Jiang, Model-guided deformable hand shape recognition without positioning aids, Pattern Recognition 38 (2005) 1651–1664.

3. S. Gonzalez, C. Travieso, J. Alonso, M. Ferrer, Automatic biometric identification system by hand geometry, in: IEEE 37th Annual International Carnahan Conference on Security Technology, 2003, pp. 281–284.

4. N. Duta, A. Jain, K. Mardia, Matching of palmprint., Pattern Recognition Letters 23 (4) (2001) 477–485.

5. X. Wu, D. Zhang, K. Wang, Fusion of phase and orientation information for palmprint authentication, Pattern Anal. Appl. (PAA) 9 (2-3) (2006) 103-111.

6. E. Yörük, E. Konukoglu, B. Sankur, J. Darbon, Shape-based hand recognition, IEEE Trans. on Image Processing 15 (7) (2006) 1803–1815.

7. C. Travieso, J. Alonso, S. David, M. Ferrer, Optimization of a biometric system identification by hand geometry, in: Complex systems intelligence and modern technological applications (CSIMTA'04), 2004, pp. 581–586.

8. A. Kumar, D. Wong, H. Shen, A. Jain, Personal authentication using hand images, Pattern Recognition Letters 27 (2006) 1478–1486.

9. S. Malassiotis, N. Aifanti, M. G. Strintzis, Personal authentication using 3-D finger geometry, IEEE Trans. on Information Forensics and Security 1 (1) (2006) 12–21.

10. G. Zheng, C.-J. Wang, T. E. Boult, Application of Projective Invariants in Hand Geometry Biometrics, IEEE Trans. on Information Forensics and Security 2 (4) (2007) 758–768.

11. O. Ghitza, Robustness against noise: the role of timing-synchrony analysis, in: 1987 IEEE International Conference on Acoustics, Speech, and Signal Processing (ICASSP '87), 1987, pp. 2372–2375.

12. C. Oden, A. Ercil, B. Buke, Combining implicit polynomials and geometric features for hand recognition, Pattern Recognition Letters 24 (2003) 2145–2152.

13. G. Boreki, A. Zimmer, Hand geometry: a new approach for feature extraction, in: Fourth IEEE Workshop on Automatic Identification Advanced Technologies (AUTOID2005), 2005, pp. 149–154.

14. A. Wong, P. Shi, Peg-free hand geometry recognition using hierarchical geometry and shape matching, in: IAPR Workshop on Machine Vision Applications (MVA02), 2002.

15. G. Amayeh, G. Bebis, A. Erol, M. Nicolescu, Peg-Free Hand Shape Verification Using High Order Zernike Moments Amayeh, in: Conference on Computer Vision and Pattern Recognition Workshop, 2006.

16. Sonka, Hlavac, Boyle, Image Processing, Analysis and Machine Vision, Chapman & Hall, 1994.

17. S. Theodoridis, K. Koutroumbas, Pattern Recognition, Academic Press, 1999.

18. SCILAB Group, at http://www.scilab.org/ (jan 2007).